ORIGINAL ARTICLE

Journal of Anatomy

ANATOMICAL SOCIETY WILEY

# Three-dimensional visualization and quantitative analysis of embryonic and fetal thigh muscles using magnetic resonance and phase-contrast X-ray imaging

Yutaka Yamaguchi[1] | Ami Murase[2] | Ryota Kodama[2] | Akira Yamamoto[3] | Hirohiko Imai[4] | Akio Yoneyama[5] | Shigehito Yamada[1,2]

[1]Congenital Anomaly Research Center, Kyoto University Graduate School of Medicine, Kyoto, Japan

[2]Human Health Sciences, Kyoto University Graduate School of Medicine, Kyoto, Japan

[3]Medical Education Center, Kyoto University, Kyoto, Japan

[4]Department of Systems Science, Graduate School of Informatics, Kyoto University, Kyoto, Japan

[5]Beamline Group, SAGA Light Source, Saga, Japan

**Correspondence**
Yutaka Yamaguchi, Congenital Anomaly Research Center, Kyoto University Graduate School of Medicine, Kyoto 606-8501, Japan.
Email: yamaguchi@cac.med.kyoto-u.ac.jp

## Abstract

The musculoskeletal system around the human hip joint has acquired a suitable structure for erect bipedal walking. However, little is known about the process of separation and maturation of individual muscles during the prenatal period, when muscle composition is acquired. Understanding the maturation process of the normal musculoskeletal system contributes to elucidating the acquisition of bipedal walking in humans and to predicting normal growth and detecting congenital muscle disorders and anomalies. In this study, we clarify the process of thigh muscle maturation from the embryonic stage to the mid-fetal stage using serial sections, phase-contrast X-ray computed tomography, and magnetic resonance imaging. We also provide a 4D atlas of human thigh muscles between 8 and 23 weeks of gestation. As a result, we first show that muscle separation in the lower thigh tends to progress from the superficial to the deep layers and that all musculoskeletal components are formed by Carnegie Stage 22. Next, we show that femur and muscle volume grow in correlation with crown-rump length. Finally, we show that the anterior, abductor, and posterior muscle groups in the thigh contain a high percentage of monoarticular muscle volume by the end of the embryonic period. This ratio approaches that of adult muscle composition during normal early fetal development and is typical of bipedal walking. This study of fetal muscle composition suggests that preparation for postnatal walking may begin in early fetal period.

**KEYWORDS**
3D reconstruction, human fetus, Kyoto collection, limb development, thigh muscle

## 1 | INTRODUCTION

Erect bipedal walking is one of the most unique human characteristics, and it is considered that humans acquire a different lower limb musculoskeletal system (MSS) from that of other primates (Ishida, 1972; Ito, 1996). However, the maturation process of this system and the acquisition of its movements during the development process are yet to be clarified. Precursory locomotor movements are exhibited during the fetal and neonatal periods, and normal prenatal musculoskeletal development is known to be stimulated by mechanical forces generated by active fetal movements (Nowlan, 2015).

Currently, fetal morphology and movement can be assessed using three-dimensional (3D) and four-dimensional (4D) ultrasonography; thereby, quantification of fetal activity (such as the timing and frequency of movements throughout development) is becoming more widespread (Lu et al., 2016). Previous studies have shown that fetal movements are first observed between 7- and 8.5-week postmenstrual age (PMA). Movements of the limbs, trunk, and head are

rapid but smooth in appearance at 10- to 12-week PMA (Lüchinger et al., 2008). Vertebrate MSS morphogenesis has been elucidated through experiments with chicks and mice (Buckingham et al., 2003; Christ & Brand-Saberi, 2002; Tickle, 2015). Muscle precursor cells in the limbs are derived from the hypaxial domains of somites, and they migrate to the limb bud area through signaling. The cells form limb muscle masses around the bone primordium, and these masses separate into individual skeletal muscles along with the development of the lower limbs a few days after the upper limbs. Muscle maturation proceeds from proximal muscles to distal muscles and is completed by the end of embryonic period, or Carnegie Stage (CS) 23 in humans (Diogo et al., 2019; O'Rahilly & Gardner, 1975).

Two-dimensional (2D) analytical approaches, such as histological sections, do not allow interpretation of complex 3D structure changes and the interaction between individual limb elements in 3D space. Mouse 3D models of lower limb muscle development are available (Delaurier et al., 2008). In recent years, several musculoskeletal studies have also been conducted using human embryos. Warmbrunn et al. (2018) reconstructed detailed 3D models of each organ at CS23 from serial sections, including muscles. They found that several individual muscle groups develop earlier or later than described in the current literature. Diogo et al. (2019) used whole-mount immunostaining embryonic images to visualize the muscles down to the tips of the limbs. They observed several atavistic muscles in human embryonic limbs, which are present in our ancestors but are normally absent in adult humans. In addition, Wilde et al. (2021) provided an anatomical description of the upper limb muscles of human embryos between CS18 and 22 using optical projection tomography. These studies show the importance of visualizing the MSS in 3D or 4D to study its maturation in more detail. Furthermore, understanding embryonic developmental processes is of interest because morphological changes during ontogeny may reflect evolutionary changes. Therefore, we consider it of importance to analyze the development of the lower-limb MSS using 3D or 4D techniques.

In recent decades, visualization of biological structures has advanced significantly in terms of both hardware and software. Since the 1990s, magnetic resonance imaging (MRI) has promoted the acquisition of detailed 3D images of relatively small embryos, including those of mammals (Pooh et al., 2011; Smith et al., 1994, 1996). Although magnetic resonance (MR) images do not provide enough resolution to observe morphological changes at the cellular level, they can show internal structures without destroying the human embryo. Matsuda et al. (2007) developed a super-parallel MR microscope equipped with 2.34 T and acquired T1-weighted images of 1204 embryos with a sufficiently high resolution of 40–150 μm$^3$. In our previous studies, 3D models of the human brain from the embryonic stage to the mid-fetal stage were reconstructed using MR images from 2.34 T, 3 T, and 7 T MR instruments (Yamaguchi et al., 2018). More recently, phase-contrast X-ray computed tomography imaging (PCXI) technology based on crystal X-ray interferometry has also been developed for the non-destructive imaging of the inner structures of mammals (Kanahashi et al., 2016; Yoneyama et al., 2011). In

PCXI, X-rays are used as electromagnetic waves that provide information regarding the amplitude and phase. When an X-ray passes through a sample, its amplitude decreases, and its phase shifts. In this method, the phase shift is directly detected by the superposition of waves, and very small differences in density in soft materials can be captured, including in embryos. In addition, advances in 3D analysis tools, such as Image J (Schneider et al., 2012), Amira software (Stalling et al., 2005), and 3D slicer (Fedorov et al., 2012) have made image analysis more accessible. Therefore, a detailed 3D model of the embryonic lower limb MSS can be reconstructed using these techniques.

The present study aimed to further characterize the morphological changes that occur in thigh muscles, from the embryonic to the fetal stage, using a recently developed imaging technique. Thigh muscle maturation during the embryonic stage was recorded three-dimensionally using phase-contrast X-ray computed tomography (PCX) images, and serial sections of the tissues were prepared for comparative purposes. Further maturation during the fetal stage was analyzed three-dimensionally and quantitatively using MRI. Based on these results, we created 4D atlases that allowed us to observe the separation and development of thigh muscles from the late embryonic stage to the fetal stage.

## 2 | MATERIALS AND METHODS

### 2.1 | Specimens

In this study, we focused on the late embryonic to mid-fetal period (Table 1), when the MSS is developing and movement of the fetus occurs. Forty-three formalin-fixed embryo and fetus specimens ranging from 15.9 mm to 225 mm in crown-rump length (CRL) were selected to observe the internal structure and reconstruct 3D models. In addition, we observed 15 sets of serial sections of embryos ranging from 14.8 to 26 mm in CRL (CS19 to CS23) to compare how well the MR and PCX images show the MSS (Figure 1, Figure S1). These human embryos are historical specimens collected and stored at the Congenital Anomaly Research Center of Kyoto University (Nishimura et al., 1968; Yamaguchi & Yamada, 2018). Over 45,000 human embryo and fetus specimens have been accumulated in the Kyoto Collection, and approximately 20% of the specimens in the collection are undamaged and well preserved. In most cases, specimens were collected after artificial abortion during the first trimester of pregnancy in accordance with the Maternity Protection Act of Japan. The use of human embryo and fetal specimens in this study was approved by the ethics committee of the Kyoto University Faculty and Graduate School of Medicine (R0316, R0347).

### 2.2 | Image acquisition

In this study, three modalities were used to observe the process of muscle maturation: PCXI, 3 T MRI, and 7 T MRI. Serial sections of

**TABLE 1** Metadata of human embryos and fetuses.

| Specimen ID | CRL (mm) | GA (day) | Carnegie stage | Sex | Right/ left leg | Femur length (mm) | Femur volume (mm³) | No. in Figure 5 |
|---|---|---|---|---|---|---|---|---|
| (PCX-CT) | 6 specimens | | | | | | | |
| 28,166 | 15.9 | 81 | Embryo (CS18) | - | Right | - | - | |
| 31,686 | 16.5 | 61 | Embryo (CS19) | - | Right | - | - | |
| 24,649 | 18.1 | 59 | Embryo (CS20) | - | Right | - | - | |
| 26,546 | 20.3 | 60 | Embryo (CS21) | - | Right | - | - | |
| 32,163 | 23.1 | 73 | Embryo (CS22) | - | Right | - | - | |
| 29,137 | 28.2 | 67 | Embryo (CS23) | - | Right | - | - | |
| (7 T MRI) | 19 specimens | | | | | | | |
| 35,233 | 21.3 | 56 | Embryo (CS22) | - | Left | 2.53 | 0.67 | 1 |
| 30,809 | 24.5 | 66 | Embryo (CS22) | - | Left | 2.73 | 0.85 | 2 |
| 24,001 | 24.6 | 69 | Embryo (CS22) | - | Left | 2.66 | 0.62 | 3 |
| 52,817 | 23.4 | - | Embryo (CS23) | - | Left | 3.33 | 1.44 | 4 |
| 25,796 | 26.8 | 84 | Embryo (CS23) | - | Left | 3.95 | 1.42 | 5 |
| 15,919 | 30.7 | 76 | Embryo (CS23) | - | Right | 4.93 | 2.15 | 6 |
| 51,397 | 32 | 75 | Embryo (CS23) | - | Right | 4.65 | 2.28 | 7 |
| 92,310 | 33.5 | 71 | Embryo (CS23) | - | Left | 5.05 | 2.48 | 8 |
| 34,509 | 34 | 78 | Fetus | - | Right | 4.8 | 2.01 | 9 |
| 52,002 | 37.2 | 104 | Fetus | - | Right | 6.23 | 4.26 | 10 |
| 33,467 | 38.7 | 118 | Fetus | Female | Left | 6.83 | 4.82 | 11 |
| 52,730 | 40 | 71 | Fetus | - | Right | 7.27 | 5.86 | 12 |
| 92,307 | 43 | 75 | Fetus | Female | Right | 8.32 | 7.38 | 13 |
| 92,038 | 43 | 91 | Fetus | Female | Left | 10.32 | 12.6 | 14 |
| 34,365 | 52.3 | 107 | Fetus | Male | Right | 9.54 | 13.6 | 15 |
| 92,214 | 69 | 95 | Fetus | Male | Right | 14.55 | 36.41 | 16 |
| 91,088 | 75 | 103 | Fetus | Female | Left | 16.48 | 56.48 | 17 |
| 92,949 | 84.5 | 63 | Fetus | Female | Left | 22.7 | 151.75 | 18 |
| 50,673 | 87 | 124 | Fetus | Male | Left | 20.45 | 133.09 | 19 |
| (3 T MRI) | 18 specimens | | | | | | | |
| 53,514 | 89 | - | Fetus | Female | Left | 20.753 | 110.71 | 20 |
| 53,216 | 105 | 110 | Fetus | Female | Left | 26.603 | 231.79 | 21 |
| 53,441 | 110 | 111 | Fetus | Female | Left | 26.43 | 251.15 | 22 |
| 53,502 | 112 | 119 | Fetus | Male | Left | 24.65 | 208.86 | 23 |
| 53,273 | 122.7 | 120 | Fetus | Male | Left | 25.28 | 241.39 | 24 |
| 53,449 | 125 | 114 | Fetus | Male | Left | 32.003 | 482.56 | 25 |
| 53,605 | 131.5 | - | Fetus | Male | Left | 33.03 | 583.14 | 26 |
| 53,598 | 143 | - | Fetus | - | Left | 36.773 | 706.55 | 27 |
| 91,517 | 148 | 136 | Fetus | Female | Right | 37.76 | 843.8 | 28 |
| 53,471 | 163 | 138 | Fetus | Male | Left | 38.62 | 940.15 | 29 |
| 53,590 | 170 | 138 | Fetus | Female | Left | 39.276 | 1177.68 | 30 |
| 53,516–2 | 170 | 130[※1] | Fetus | - | Left | 42.44 | 1080.61 | 31 |
| 93,226 | 175 | 141[※2] | Fetus | Male | Left | 42.86 | 1227.74 | 32 |
| 53,467 | 185 | 134[※1] | Fetus | Female | Right | 43.75 | 1263.45 | 33 |
| 53,595 | 190 | - | Fetus | Female | Left | 46.183 | 1754.21 | 34 |
| 53,513 | 198 | 154 | Fetus | Female | Left | 42.886 | 1436.68 | 35 |
| 53,588 | 205 | 157 | Fetus | Male | Left | 52.71 | 2297.74 | 36 |
| 53,570 | 225 | 151[※1] | Fetus | Male | Left | 55.78 | 2766.22 | 37 |

**TABLE 1** (Continued)

| Specimen ID | CRL (mm) | GA (day) | Carnegie stage | Sex | Right/ left leg | Femur length (mm) | Femur volume (mm$^3$) | No. in Figure 5 |
|---|---|---|---|---|---|---|---|---|
| (Serial sections) | 15 sets | | | | | | | |
| 3874 | 14.8 | 56 | Embryo (CS19) | - | Left | - | - | |
| 32 | 15 | 59 | Embryo (CS19) | - | Left | - | - | |
| 7778 | 16.4 | 80 | Embryo (CS19) | - | Left | - | - | |
| 16,264 | 18 | 59 | Embryo (CS20) | - | Left | - | - | |
| 4330 | 18.6 | 65 | Embryo (CS20) | - | Right | - | - | |
| 10,344 | 19.1 | 56 | Embryo (CS20) | - | Left | - | - | |
| 16,393 | 18.7 | 59 | Embryo (CS21) | - | Right | - | - | |
| 2021 | 21.4 | 64 | Embryo (CS21) | - | Left | - | - | |
| 2314 | 22.6 | 80 | Embryo (CS21) | - | Right | - | - | |
| 10,642 | 18.9 | 59 | Embryo (CS22) | - | Right | - | - | |
| 12,246 | 21.2 | - | Embryo (CS22) | - | Left | - | - | |
| 15,768 | 22.8 | - | Embryo (CS22) | - | Left | - | - | |
| 9026 | 25.7 | 66 | Embryo (CS23) | - | - | - | - | |
| 10,273 | 27.5 | 62 | Embryo (CS23) | - | Right | - | - | |
| 9005 | 26 | 80 | Embryo (CS23) | - | - | - | - | |

*Note*: List of specimens used in this study. All specimens used in this study were fixed specimens. For some specimens, there were no data on the exact date of the last menstrual period. In addition, some specimens had inappropriate gestational ages affected by irregular menstrual cycles of their mothers. There is a margin of error of approximately 14 days in *1 and approximately 7 days in *2. In the embryonic and early fetal stages, external genitalia are undifferentiated, and sex determination is not possible from the external surface; therefore, only specimens whose sex could be determined from the external surface are described. All serial sections were obtained at 10 μm thickness and stained with hematoxylin and eosin.

whole embryos were used for comparative purposes during early stages of development.

The PCX images were acquired using a PCXI system fitted with a crystal X-ray interferometer. The system was set up at the vertical wiggler beamline of the Photon Factory of the High-Energy Accelerator Research Organization. A skew-symmetric two-crystal X-ray interferometer was used to detect the phase shift that occurs when the X-rays pass through a sample. More details on the PCXI image acquisition conditions have been provided in previous studies (Yoneyama et al., 2011). Thus, 3D embryonic images with a pixel size of 6.5 μm$^3$ were acquired. These images were binned during the image processing process and used as images with a pixel size of 13 μm$^3$. Due to equipment restrictions, PCXI was used for specimens of approximately 25 mm or less in the CRL. In some cases, only the lower extremities were imaged using PCXI in the larger embryos.

MR images were acquired by using a 7 T MR system (BioSpec 70/20 USR; Bruker BioSpin MRI GmbH) and a 3 T MR system (MAGNETOM Prisma; Siemens Healthineers). The spatial resolution of each was 35.4–109.4 μm$^3$ on 7 T MRI and 100–200 μm$^3$ on 3 T MRI. In this study, we used these different methods depending on the size of the specimens due to the size of the MR coil; the 7 T MR system was used to acquire 3D images of embryonic specimens larger than CRL 25 mm and fetal specimens smaller than CRL 90 mm, while the 3 T MR system was used for fetal specimens with a CRL larger than 90 mm. The specimens obtained using PCXI and MRI

were then stabilized in suitably sized containers filled with approximately 0.65%–1% agarose gel.

Serial sections used to confirm the findings of 3D imaging modalities have already been obtained at 10 μm thickness and stained with hematoxylin and eosin (Yamaguchi & Yamada, 2018). Each slice was digitalized at 20× magnification using an Olympus virtual slide system (VS120-S5-J; Olympus Corp.,) and cropped using ImageJ software.

## 2.3 | Three-dimensional reconstruction and analysis

In this study, two main processes were analyzed: the muscle separation process around the hip joint during the embryonic period, and the muscle maturation process in the thigh during the fetal period.

The muscle separation process was observed using PCX images of human embryonic specimens up to 8- to 10-week gestational age (GA: same as PMA in this study) (CS18-CS23), and results were compared with serial sections. The target muscles were anatomically classified into five groups: anterior muscles (rectus femoris, vastus medialis, vastus intermedius, vastus lateralis, and sartorius), posterior muscles (biceps femoris long head, biceps femoris short head, semitendinosus, and semimembranosus), medial muscles (pectineus, gracilis, external obturator, adductor magnus, adductor longus,
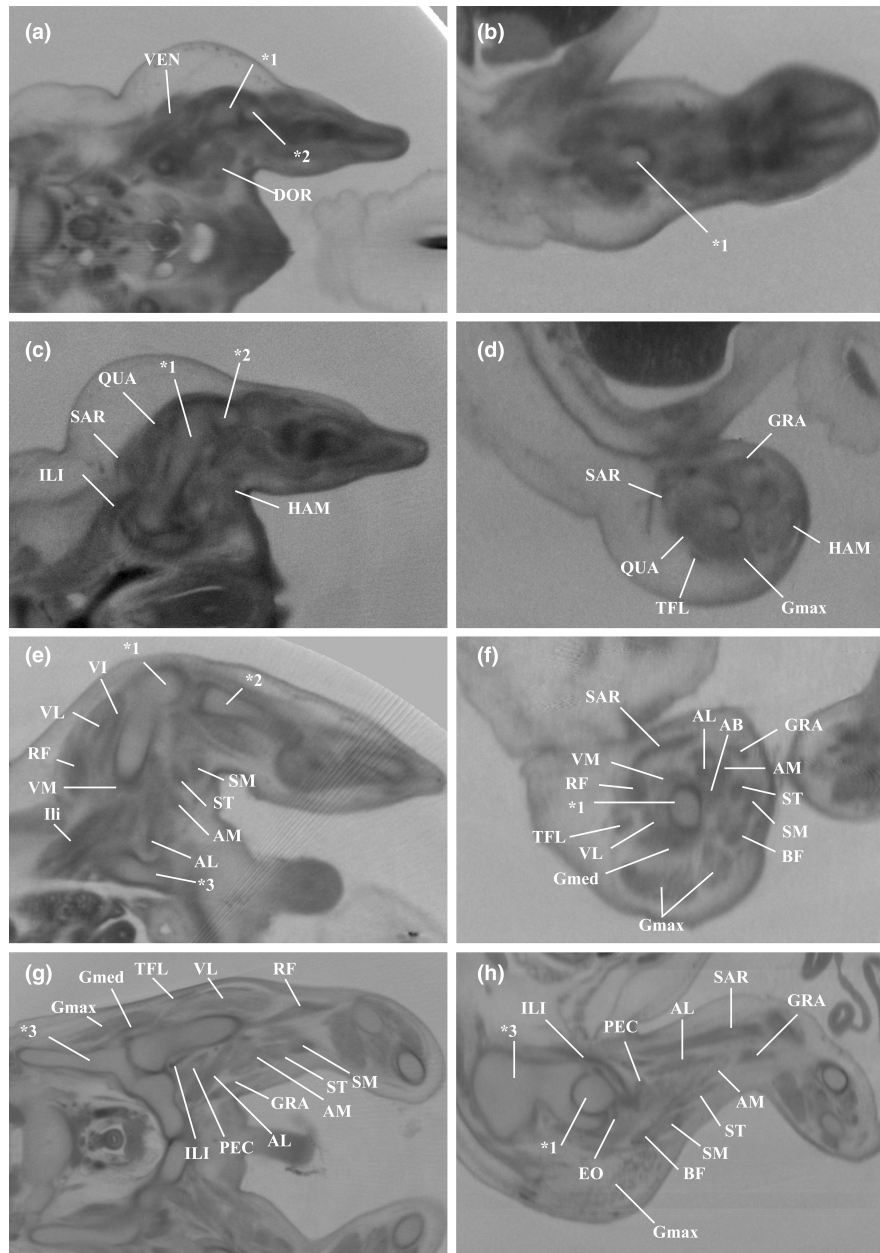
**FIGURE 1** Right lower limb images obtained using phase-contrast X-ray computed tomography imaging. The horizontal and sagittal views are shown in CS18, 19, 21, and 23. (a, b): CS18; (c, d): CS19; (e, f): CS21; (g, h): CS23. At CS18, VEN and TIB could be observed around the femur, but they could not be segmented into individual muscles. From CS19, separation of the superficial muscles progressed, and at CS21, approximate segmentation of the thigh muscles was possible. Later, the gluteal muscle group was also separated, and positioning of the muscles around the hip joint was complete by CS23. *1, Femur; *2 Tibia; *3, Coxae; AL, adductor longus; AM, adductor magnus; CS, Carnegie stage; DOR, dorsal muscle mass; Gmax, gluteus maximus; Gmed, gluteus medius; GRA, gracilis; HAM, hamstrings; ILI, iliopsoas muscles; PEC, pectineus; QUA, quadriceps; RF, rectus femoris; SAR, sartorius; SM, semimembranosus; ST, semitendinosus; VEN, ventral muscle mass; VI, vastus intermedius; VL, vastus lateralis; VM, vastus medialis.

and adductor brevis), iliopsoas muscles (psoas major and iliacus), and gluteal muscles (tensor fasciae latae, gluteus maximus, gluteus medius, and gluteus minimus) (Table 2). Based on these classifications, the PCX images were manually segmented using the 3D visualization and analysis software Amira (VSG Corp, V.6.0.1, V.6.5.0, Visualization Science) (Figure 2). In addition, the timing of tendon attachment (which was difficult to observe due to imaging resolution) was based on serial section observations (Figure S2).

Next, the maturation process of MSS in the thigh was analyzed using 3 T and 7 T MRI. The 3D models of these muscles were reconstructed using Amira software. Based on these muscle models, thigh muscle volume and femur and leg length were measured three times, and the average value was calculated. The correlation coefficients were calculated using the CORREL method. Additionally, thigh muscle composition during fetal development was comparison to that of human adults (Charles et al., 2019) as well as gorillas and orangutans (Zihlman et al., 2011).

TABLE 2  Identification of nascent muscles during late Carnegie stages.

| | Muscle | Abbreviation | CS18 | CS19 | CS20 | CS21 | CS22 | CS23 |
|---|---|---|---|---|---|---|---|---|
| Anterior muscle Group | Sartorius | SAR | | ▓ | ▓ | ▓ | ▓ | ▓ |
| | Rectus femoris | RF | | | ▓ | ▓ | ▓ | ▓ |
| | Vastus lateralis | VL | | | | ▓ | ▓ | ▓ |
| | Vastus intermedius | VI | | | | ▓ | ▓ | ▓ |
| | Vastus medialis | VM | | | ▓ | ▓ | ▓ | ▓ |
| Iliopsoas | Iliopsoas | ILI | | | | ▓ | ▓ | ▓ |
| Medial muscle Group | Pectineus | PEC | | | | ▓ | ▓ | ▓ |
| | Adductor magnus | AM | | | | ▓ | ▓ | ▓ |
| | Adductor longus | AL | | | | ▓ | ▓ | ▓ |
| | Adductor brevis | AB | | | | ▓ | ▓ | ▓ |
| | External obturator | EO | | | | ▓ | ▓ | ▓ |
| | Gracilis | GRA | | | ▓ | ▓ | ▓ | ▓ |
| Posterior muscle Group | Biceps femoris | BF | | | ▓ | ▓ | ▓ | ▓ |
| | Semitendinosus | ST | | | ▓ | ▓ | ▓ | ▓ |
| | Semimembranosus | SM | | | ▓ | ▓ | ▓ | ▓ |
| Gluteus muscle Group | Gluteus maximus | Gmax | | | | ▓ | ▓ | ▓ |
| | Gluteus medius | Gmed | | | | | ▓ | ▓ |
| | Gluteus minimus | Gmin | | | | | ▓ | ▓ |
| | Tensor fasciae latae | TFL | | ▓ | ▓ | ▓ | ▓ | ▓ |

*Note*: The timing of muscle separation was confirmed using both phase-contrast X-ray computed tomography and serial sectioning. White boxes indicate stages where individual muscles had not yet separated from the muscle mass, and gray boxes indicate stages where muscle separation is complete.

## 3 | RESULTS

### 3.1 | Thigh muscle separation

The entire process of individual muscle maturation from CS18 to CS23 is shown in Figures 1, 3, S3 and Table 2. At CS18, some masses of primitive muscle fibers were observed around the primordium of the femur, but they could not be separated into individual muscles (Figure 1). At CS19, some individual muscles began to form from the muscle mass (Figure 1, 3a,b), and the separation of all targeted muscles was confirmed after CS22 (Figure 3g,h). The thigh muscles tended to separate into individual muscles earlier than the gluteal muscles did. Comparisons between the thigh muscle groups showed a general trend; medial muscle group development was the slowest, and superficial muscles, such as the gracilis or sartorius, formed in earlier stages than deep muscles. In the PCX-CT images, the separation of the muscle belly and serial sections within the target muscle could be confirmed, but tendon attachment was difficult to distinguish. Therefore, tendon attachment timing was observed using serial sections (Figure S2, Table 3).

In addition, 3D models of the lower thigh muscles from 21.3 mm (CS22 embryo) to 225 mm of CRL were reconstructed using MR images (Figure S4). Quadriceps, sartorius, gracilis, and adductor magnus were discriminated in all specimens. On the other hand, in some specimens, the vastus muscle groups, adductor longus and brevis, and hamstrings could not be individually segmented because of the low resolution of MRI, although they were already separated histologically in embryonic periods.

### 3.2 | Anterior muscles

The sartorius was the first to separate in the anterior muscle group, followed by the rectus femoris and vastus muscle groups. At CS19, the sartorius was almost completely separated from the muscle mass and formed a flattened structure distal to the medial thigh. In contrast, the quadriceps femoris was a muscle mass that was not well separated (shown as "vastus muscle group" in Figure 3b), and the distal part of the gluteus muscle group was not yet completely separated (Figure 3a,b). The proximal part of the rectus femoris began to separate at CS19 (not shown in Figure 3a,b); however, there was no attachment to the ilium primordium. At CS20, quadriceps femoris separation was confirmed after the sartorius, and the origin of the rectus femoris was attached to the ilium primordium (Figure 3c, Table 3). In the vastus muscle group, the medial side separated faster than the lateral side, and the vastus medialis could be extracted (Figure 3d). Separation of the vastus lateralis and vastus intermedius was observed at CS21 (Figure 3e,f). The sartorius elongated in both the origin and insertion directions during developmental progression, attaching to the anterior superior iliac spine of the ilium
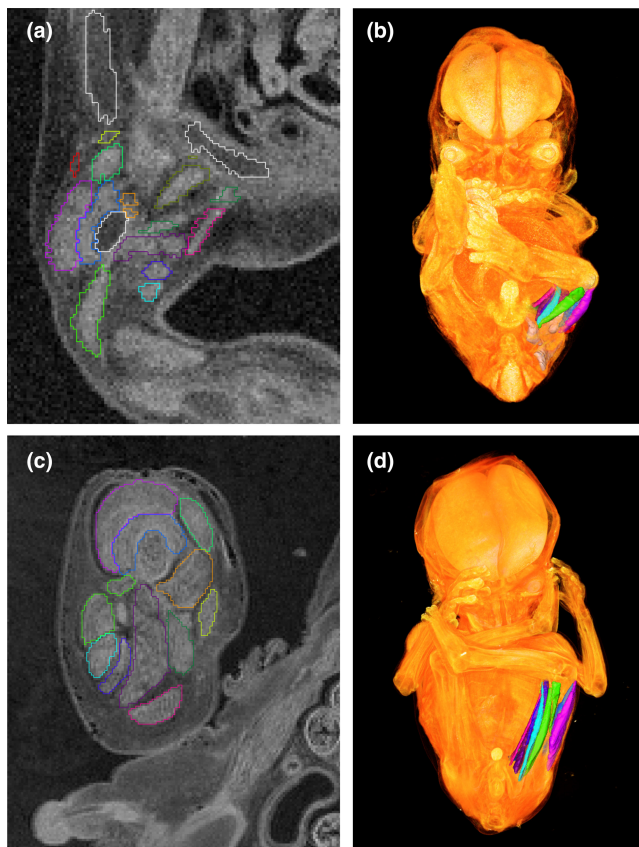
**FIGURE 2** Segmentation of musculoskeletal system components. (a, c): A 7 T magnetic resonance image of an early fetus. (b, d): Musculoskeletal system model reconstructed using Amira software. (a, b): CRL 21.3 mm (8-week GA). (c, d): CRL 43 mm (13-week GA). The color codes are the same as in Figure 3.

and to the tibia primordium during CS21 and CS23 (Figure 3d,f,h,j, Table 3) and continuing to elongate thereafter. At CS22, the patellar primordium appeared on the distal tendon of the quadriceps femoris, and the elements of the anterior muscles were then completed (Figure 3g,h).

### 3.3 | Medial muscles and iliopsoas muscle

In the medial muscle group, the gracilis was first observed as a small and flat muscle concentrated in the proximal medial thigh, while other medial muscles were observed as a relatively small muscle mass on the medial side of the thigh at CS19 (Figure 3b). In addition, a large muscle mass extending from the lumbar region was observed in the iliopsoas (Figure 3b). Although the origin could be separated into the iliacus and psoas, the distal part merged and attached to the femoral primordium. At CS20, two muscle masses were observed medial to the gracilis. One was the adductor magnus, and the other was the mass of the other medial muscles (Figure 3d). The latter was separated into the adductor longus, adductor brevis, and external obturator at CS21 (Figure 3f). At the same stage, the pectineus appeared to separate

from the iliopsoas and was observed above the medial muscle group. The gracilis with its flattened structure, as well as the sartorius, extended toward both origins as they progressed through the developmental stages, and the gracilis tendon was attached to the tibial primordium during CS21 and CS23 (Figure 3b,d,f,h,j, Table 3).

### 3.4 | Posterior muscles

The distal part of hamstrings was more separated from the muscle mass than proximal part at CS19 (Figure 3a). In addition, the origin of the short head of the biceps femoris was observed at this stage. At CS20, the separation of the hamstrings progressed, and individual muscles could be observed (Figure 3c,d). At CS21, the boundaries of the individual muscles became apparent, and the tendon of each muscle was attached between CS21 and CS22 (Figure 3f,h, Table 3).

### 3.5 | Gluteal muscles

The gluteal muscles separated from the muscle mass between CS19 and CS20 (Figure 3a,c). At CS19, the gluteus maximus was observed almost in isolation, but, distally, it was connected to the lateral side of the vastus muscles. On the medial side of the gluteus maximus, there were masses of the gluteus medius and gluteus minimus (shown as the color "gluteus medius" in Figure 3a), which were still continuous with the vastus muscles (Figure 3a). In contrast, the tensor fasciae latae was well-separated and could be observed as an independent muscle after CS19. During CS22, the gluteus medius and gluteus minimus were separated, and the boundaries of the individual muscles became apparent at CS23 (Figure 3i).

In addition, the gluteus maximus showed the greatest change in position among all muscles. At CS19, the gluteus maximus extended perpendicular to the long axis of the femur (Figure 3a), and the muscle mass was separated into upper and lower fibers at CS20 (Figure 3c). The space between them closed between CS20 and CS21 (Figure 3c,e), and after CS21, the muscle ran along the long axis of the femur as the developmental stage progressed (Figure 3e,g,i).

### 3.6 | Changes in thigh muscle volume

Next, we quantitatively analyzed how the thigh muscles changed during development based on the 3D models as reconstructed from the MR images (Figure S4). The volume of each muscle and the femur length were measured and compared between specimens after CS22 (CRL 21.3 mm and larger), when the separation of target muscles around the hip joint was completed.

Figure 4 shows the relationship between femoral variables, thigh muscle volume, and CRL. The correlation between femur

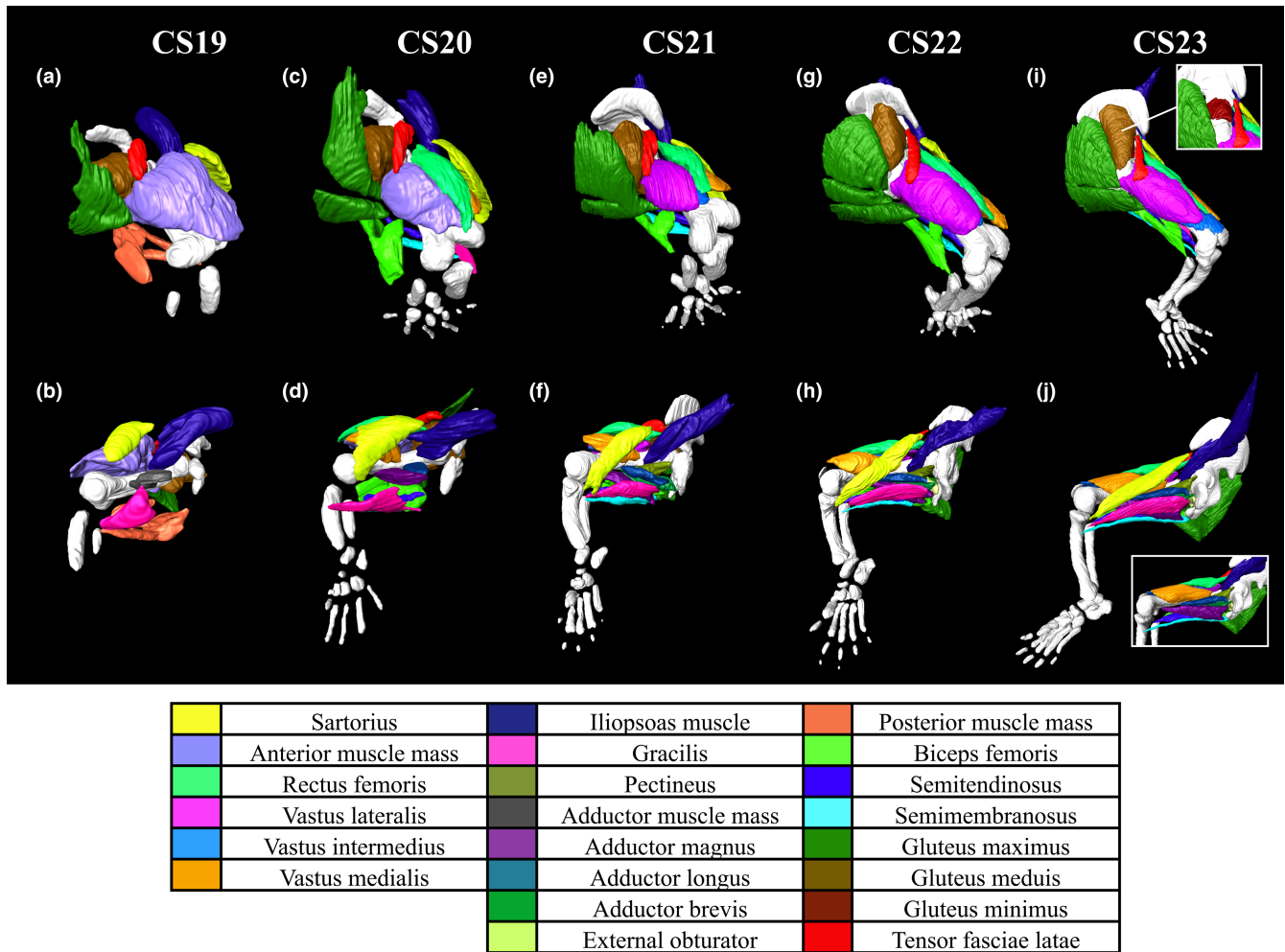| | | | |
|---|---|---|---|
| Sartorius | Iliopsoas muscle | Posterior muscle mass |
| Anterior muscle mass | Gracilis | Biceps femoris |
| Rectus femoris | Pectineus | Semitendinosus |
| Vastus lateralis | Adductor muscle mass | Semimembranosus |
| Vastus intermedius | Adductor magnus | Gluteus maximus |
| Vastus medialis | Adductor longus | Gluteus meduis |
| | Adductor brevis | Gluteus minimus |
| | External obturator | Tensor fasciae latae |

**FIGURE 3** The 3D reconstructed models of embryonic lower limbs. Samples were taken at Carnegie stage (CS) 19 to CS23 and reconstructed from phase-contrast X-ray computed tomography images. (a, b): CS19; (c, d): CS20; (e, f): CS21; (g, h): CS22; (i, j): CS23. The upper models are viewed from the superior and lateral aspects (a, c, e, g, and i), and the lower models are viewed from the medial aspects (b, d, f, h, and j). The frame in (i) shows the gluteus minimus in the deeper layers, removing the gluteus medius. The frame in (j) shows the deeper layers of the adductor muscle group, removing the sartorius and the gracilis.

**TABLE 3** Tendon attachment timing.

| Muscle | | CS19 | CS20 | CS21 | CS22 | CS23 |
|---|---|---|---|---|---|---|
| Anterior muscle group | Sartorius | − | − | + | + | ++ |
| | Rectus femoris | − | + | ++ | ++ | ++ |
| Medial muscle group | Gracilis | − | − | + | + | ++ |
| Posterior muscle group | Biceps femoris | − | + | + | ++ | ++ |
| | Semitendinosus | − | − | + | ++ | ++ |
| | Semimembranosus | − | − | + | ++ | ++ |

*Note*: Serial sections of three embryonic specimens were investigated at each stage from CS19 to CS23 to confirm tendon attachment. The specimen list is shown in Table 1, and the serial sections are shown in Figure S2. Instances, where attachment could be confirmed in only some of the specimens, were designated as +. Instances, where attachment (to both the origin and insertion) could be observed in all three specimens, were designated as ++.

length and CRL was strong ($R^2$ = 0.9888) in all 37 specimens with a CRL of 21.3 to 225 mm (Figure 4a). The relationship between (femur length)$^3$ and femur volume also showed a strong correlation ($R^2$ = 0.9914) (Figure 4b). In addition, the correlation between total thigh muscle volume and femur volume was also high ($R^2$ = 0.9874) (Figure 4c). That is, during development, the femur grows in proportion to CRL, and the balance of bone volume and muscle volume is also constant.
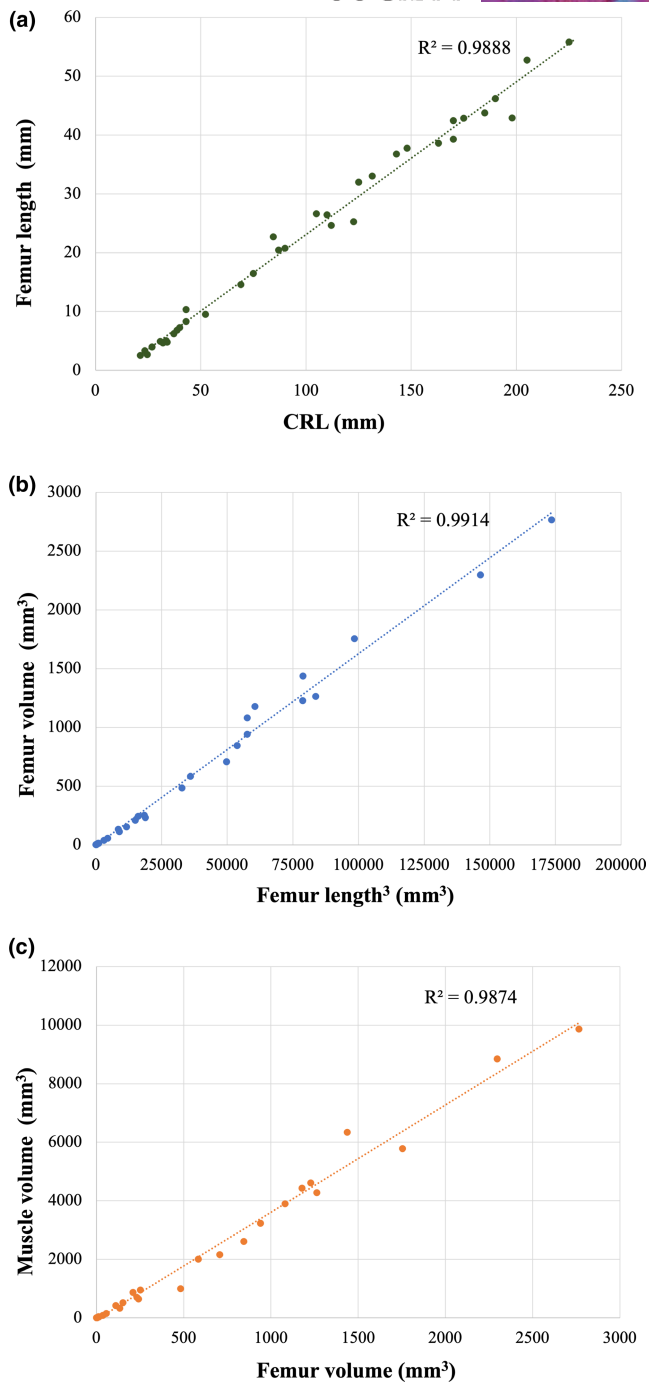
**(a)**



**(b)**



**(c)**



**FIGURE 4** Relationships between crown-rump length (CRL), femoral variables, and thigh muscles. (a) CRL and femur length; a comparison of length to length. (b) Femur length and femur volume; a comparison between length to the cube and volume. (c) Femur volume and thigh muscle volume; a comparison of volume to volume.

## 3.7 | Comparisons of muscle composition

For specimens with a CRL of 21.3–225 mm, the changes in muscle composition ratios were analyzed among and within three muscle groups (anterior muscles, medial muscles, and posterior muscles) (Figure 5). From the findings in Figure 5, it has been shown that the proportion of monoarticular muscles increases as the fetus grows (summarized in Table 4).

The ratio of muscle groups in the entire thigh of each fetus is shown in Figure 5a. The muscle volume ratio of the human fetus varied from approximately 54%–68% for the anterior muscles, from approximately 15%–26% for the adductor muscles, and from approximately 15%–24% for the posterior muscles between CRL 21.3 and 225 mm. The thigh muscle composition of adult humans has a higher proportion of anterior muscle groups and a lower proportion of medial and posterior muscle groups compared to the muscle composition of other apes (Charles et al., 2019; Zihlman et al., 2011).

In the anterior muscle group (Figure 5b), the proportion of the vastus muscles, which are monoarticular muscles, was high from the beginning of the human fetal period; in addition, there was a slight increase in the proportion of monoarticular muscles relative to that of biarticular muscles, such as the rectus femoris and the sartorius. The proportion of the rectus femoris was high in orangutans, whereas the proportion of the vastus muscles was high in adult humans.

In the medial muscle group (Figure 5c), the proportions of the gracilis decreased during the fetal period. In adult humans, the proportion of gracilis is smaller, and the proportion of adductor muscles is larger than that in great apes.

In the posterior muscle group (Figure 5d), the proportions of the biceps femoris and semitendinosus were higher in earlier fetuses, while the proportion of semimembranosus increased in later fetuses, although the tendency of change was not clearly elucidated. In adult humans, the posterior muscle group showed lower proportions of biceps femoris and semitendinosus and higher semimembranosus proportions than in apes. All of these characteristics and trends are summarized in Table 4.

## 4 | DISCUSSION

Recent advances in imaging technology have enabled the analysis of the internal structures of valuable and small specimens, such as human embryos. This study focused on the developmental process of the thigh MSS during the early fetal period, with a specific focus on morphological changes in 3D structure and composition.

In standard textbooks, the muscle primordium of the lower limb is described as forming dorsal and ventral muscle masses; the dorsal mass comprises extensor and abductor muscles, while the ventral mass consists of flexor and adductor muscles. However, they provide only brief information on morphological muscle development, and the separation process of individual muscles is often neglected. Furthermore, studies on musculoskeletal development are mainly based on findings from experiments on chicks and mice (Buckingham et al., 2003; Christ & Brand-Saberi, 2002; Tickle, 2015) and are not sufficient to discuss the process of acquiring a human-specific MSS.

In this study, we visualized developmental changes using three modalities: PCXI, 3 T MRI, and 7 T MRI. Although morphological changes are difficult to observe at the cellular level (as in serial sections or whole-mount immunostaining), they enable nondestructive
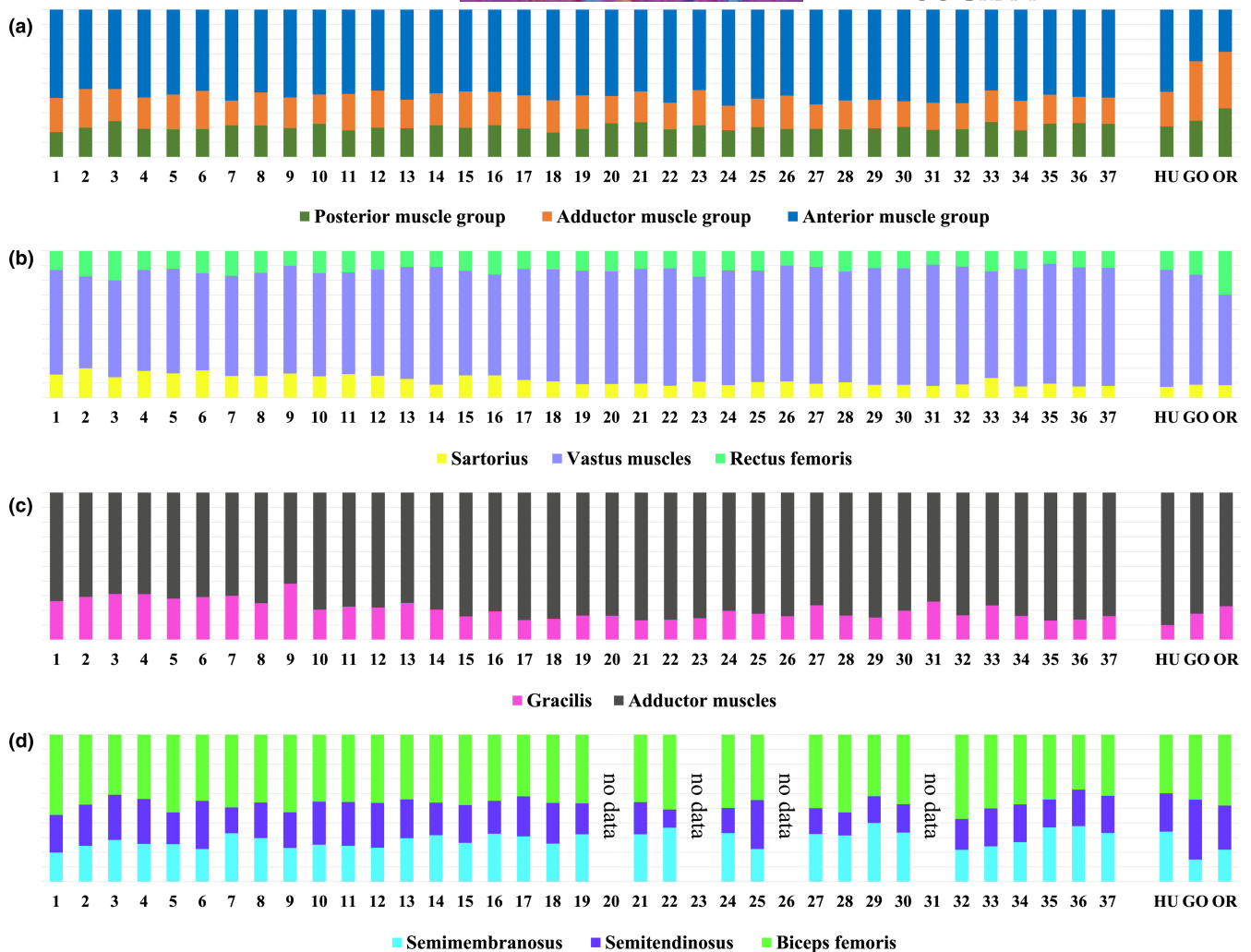
**FIGURE 5** Graphs of muscle composition. (a) Composition among the three muscle groups, (b) Composition in the anterior muscle group, (c) Composition in the medial muscle group, (d) Composition in the posterior muscle group. The number of each specimen corresponds to those in Table 1. For comparison, the average of the muscle weight ratios of HU (Charles et al., 2019), GO, and OR (Zihlman et al., 2011) are shown on the right side of each graph. In the posterior muscle group (d), the specimens from CRL90, 112, 131.5, and 170 have no data, because it was difficult to segment the hamstrings into individual muscles due to the magnetic resonance imaging resolution. GO, gorilla; HU, human (adult); OR, orange.

**TABLE 4** Characteristics and trends of fetal thigh muscle development.

| Muscle group | Characteristics and trends during development | Characteristics muscle proportions of an adult human in comparison with that of gorilla and orangutan |
|---|---|---|
| Whole thigh muscles (Figure 5a) | Mainly composed of anterior muscles. | A higher proportion of anterior muscles. |
| Anterior muscle group (Figure 5b) | Mainly composed of vastus muscles, which increased proportionally during development. | A higher proportion of vastus muscles. |
| Medial muscle group (Figure 5c) | The ratio of gracilis deceased during development. | A lower proportion of gracilis. |
| Posterior muscle group (Figure 5d) | Possible decrease in biceps femoris ratio? Possible decrease in semimembranosus ratio? | A lower proportion of biceps femoris and semitendinosus, and a higher proportion of semimembranosus muscles. |

*Note*: A summary of the data in Figure 5.

specimen analysis because of their resolution. This study was characterized by nondestructive specimen analysis and the use of multiple modalities to monitor musculoskeletal changes from the early embryonic to the mid-fetal period. The dataset generated during the current study is available from the corresponding author on reasonable request.

## 4.1 | Muscle development around the hip joint

The muscle separation process was mainly determined based on PCX images obtained with a very high resolution of 13 μm³, and serial sections at the same CS were also used for comparison (Figure 1, S1 and Table 1). Using imagery, muscle segmentation could be identified at the same stage as the serial sections (Table 2), although it was comparatively more difficult to observe muscle fibers. The PCX image at CS18 showed ventral and dorsal muscle masses around the bone primordium (Figure 1). The muscle mass appeared to begin to separate into individual muscles, but it was still difficult to distinguish the individual muscles at this stage. All thigh muscle elements separated and formed after CS18 and were completed by CS22.

Bardeen and Lewis (1901), Bardeen, 1906 previously investigated the process of limb muscle maturation based on histological sections, and Diogo et al. (2019) summarized their data. These data showed that many thigh muscles appeared in embryonic specimens with CRL of 10.5 or 12 mm (7-week GA). The specimens used in these studies were in an earlier period of development than ours, and it would seem that the results obtained from them correspondingly differed. However, in those studies, even when the muscles were not completely morphologically separated, they were classified as individual muscles. In contrast, we categorized each muscle as fully formed from the point when it was fully segmented. Therefore, a direct comparison with those studies is ill-advised, and our results are not necessarily contradictory. Moreover, our study could provide further clarification regarding the timing of individual muscle development. In addition, Nishimura et al. (1968) showed that even at the same developmental stage, there was little variation in the size of the embryos regarding the correlation between CS and CRL. CS is a stage index based on the external surface; embryo size and internal development probably differ within the same stage. Therefore, a more accurate discussion regarding the correlation between lower limb muscle development, CS, and embryo size would require further investigation with larger sample sizes.

This study showed that superficial muscles, such as the sartorius, gracilis, and tensor fasciae latae, separated earlier, and deeper muscles separated in the later stage (Figure 3, S3). This general trend was also observed in the study of human embryo forelimbs by Wilde et al. (2021). In addition, the timing of muscle tendon attachment to the bone matrix was examined. A previous study showed that the muscles, tendons, and bones of the limbs develop through interaction with each other; induction of distal limb tendons relies on signals from cartilage, and proximal tendons rely on interactions with muscles (Huang, 2017; Huang et al., 2015). However, a correlation between the timing of muscle development and muscle attachment to the bone has not been previously described. In this study, several muscles were observed, with an emphasis on the timing of muscle separation and muscle attachment to the bone primordium (Tables 2 and 3). In the anterior muscle group, attachment of the rectus femoris to the ilium was observed before muscle separation, whereas attachment of the sartorius to the ilium was confirmed

after its separation. Not all muscles were examined, because it was difficult to determine muscle attachment in PCXI and MRI due to resolution limitations and slice orientation in histological serial sections. Despite these limitations, there was no definite relationship between muscle separation and attachment; all muscles separated and attached before CS23.

Using the 3D reconstructed models from PCXI (Figure 3, S3), although most muscles did not show any significant changes in position, the gluteus maximus showed significant changes in 3D shape and direction during the developmental process. The gluteus maximus extended perpendicularly to the major axis of the femur at CS19 and parallel to the femur at CS22 (Figure 3). The gluteus maximus is a monoarticular muscle that is important for bipedal walking in humans and is more developed than in other apes. The morphology of the gluteus maximus is different between humans and other apes; it consists of two parts, proprius and ischiofemoralis in non-human apes, whereas humans have only proprius and iliotibial tracts (Lieberman et al., 2006). The gluteus maximus in chimpanzees has a relatively long muscle moment arm at the hip, with a short femur (Hogervorst & Vereecke, 2014). Additionally, the gluteus maximus insertion was more distal to the femur. This arrangement confers large extension power to ape hindlimbs, which is essential for vertical climbing. On the other hand, in humans, the gluteus maximus became larger, and the femur became longer than in non-human apes; simultaneously, the muscle moment arms were shortened, decreasing the power-generating capacity of the muscles. Such a rearrangement is suitable for generating speed during bipedal walking (Hogervorst & Vereecke, 2014). Greiner (2002) also proposed that human gluteal morphology is a consequence of upright bipedal posture. Therefore, the rearrangement of the gluteus maximus might have been significant for humans to acquire bipedalism, and the changes in the position and orientation of this muscle that occur during embryonic development may be related to evolutionary processes.

## 4.2 | Changes in muscle composition during early fetal periods

Quantitative analysis was performed on specimens after CS22, when the separation of each muscle was complete, based on 3D models reconstructed from 3 T MRI and 7 T MRI images. Femur length has been shown to correlate with estimated body weight and menstrual age in previous studies (Hadlock et al., 1982, 1984) and is already commonly used as a predictor variable of fetal weight in clinical practice. In addition, it has been shown that CRL and femur length are correlated from the embryonic to the late fetal stages (Suzuki et al., 2019; Ziylan & Murshid, 2003). In our study, there was also a strong positive correlation between femur length and CRL ranging from 21.3 to 225 mm (Figure 4a). These data provide solid support for using femur length as an indicator of fetal development in the early to mid-fetal periods, and femur length can be used as a surrogate marker for CRL in the study using fetal specimens.

Furthermore, this study showed strong positive correlations between femur length, femur volume, and thigh muscle volume in normal specimens (Figure 4b,c). The ratio of fetal size, muscle volume, and bone volume was constant, despite the period when lower-limb movements continued to increase (Figure 4). It has been suggested that biomechanical stimulation by uterine wall kicking affects the formation of the skeleton and joints (Verbruggen et al., 2018). During normal development, the nervous system and MSS develop during fetal period, resulting in limb movement. The differentiation of specific movement patterns within the 8- to 14-week GA period was hypothesized to originate supraspinally (de Vries & Fong, 2006): simple limb movements at 9- to 10-week GA (CRL 16–30 mm) and complex limb movements at 11- to 12-week GA (CRL 31–50 mm) (Kurjak et al., 2002; Lüchinger et al., 2008). In addition, a rapid increase in the number of axonal synapses in motoneurons has been confirmed at 14- and 15-week GA (Castiello & Parma, 2018). Kicking movements in the lower limbs increase substantially up to 30-week GA and decrease significantly at 35-week GA (Verbruggen et al., 2018). Previous research has also shown that the mechanical forces of fetal movement stimulate the fetal skeleton and are important for normal musculoskeletal development (Nowlan, 2015; Verbruggen et al., 2018). There is a possibility that normal development of movement and nerves leads to proportional MSS growth. This balance may be disrupted by congenital abnormalities. For example, neuromuscular disorders that result in reduced or absent fetal movement clinically result in skeletal malformations, such as joint fusions, craniofacial abnormalities, and hypomineralized bones (Aronsson et al., 1994; Rodríguez, Garcia-Alix, et al., 1988a; Rodríguez, Palacios, et al., 1988b).

Next, the timing of the acquisition of thigh muscle composition was investigated by examining changes in the muscle volume ratio during the fetal period (Figure 5, Table 4). The muscle composition characteristics of the human fetus were compared with data from studies on weight ratios in human adults (Charles et al., 2019), gorillas, and orangutans (Zihlman et al., 2011). The most significant trend observed in adult humans compared to great apes was a higher proportion of monoarticular muscles, such as the vastus muscles in the anterior muscle group and adductor muscles in the medial muscle group. Monoarticular muscles developed during the transition from arboreal to terrestrial life to support bipedalism (Ishida, 1972). In particular, the hip and knee joints are flexed during primary bipedal walking in monkeys (Okada et al., 1996), and the muscles that maintain knee and hip extension must be developed for erect bipedal walking. Therefore, monoarticular muscles are particularly important for maintaining the standing position, and the role of the vastus muscle group has increased in the thighs (Ishida, 1972). Therefore, as a result of adaptation to bipedal walking, human adults have a higher proportion of anterior thigh muscle groups (including the vastus) than the great apes.

When apes and monkeys temporarily walk on two hind limbs, the hamstrings, especially the biceps femoris, provide propulsive power, although they are biarticular muscles (Ishida, 1972). Chimpanzees have a long ischial tuberosity that creates a very effective muscle moment arm for the hamstrings in the flexed hip, resulting in a high propulsive force (Hogervorst & Vereecke, 2014). However, in the erect posture, the hamstring muscle moment arm is shorter, and the hamstrings produce less power for extension of the hindlimb. However, human ancestors have adapted their monoarticular muscles, such as the gluteus maximus, to power long-term bipedal walking, and the hamstrings have become less important as a source of propulsive force. Therefore, the proportion of hamstrings in the posterior muscle group has decreased during evolution (Hogervorst & Vereecke, 2014; Ishida, 1972). This trend was observed from the CS22 embryonic stage (21.3 mm in CRL), when the separation of each muscle was completed (Figure 5a).

In this study, the proportion of monoarticular muscles during the fetal period tended to increase in the anterior and medial muscle groups. In the posterior muscles, the proportions of the biceps femoris and semitendinosus muscles were higher in earlier fetuses, while the proportion of semimembranosus muscles increased in later fetuses, although the tendency was not definitely proven. One of the reasons for this is the MRI resolution; it was difficult to distinguish between the semitendinosus and semimembranosus muscles. More cases using higher-resolution images would clarify the posterior muscle group variance during the fetal period. The anterior, abductor, and posterior muscle groups in the thigh contain a high percentage of monoarticular muscle volume by the end of the embryonic period. This ratio approaches that of adult muscle composition during normal early fetal development and is typical of bipedal walking (Figure 5, Table 4). This study of fetal muscle composition suggests that the thigh muscle balance suitable for bipedal walking is programmed from the early fetal period, not after birth.

## 5 | CONCLUSION

In recent years, 3D analysis of embryos and fetuses using reconstructed models has attracted attention. In this study, we performed non-destructive 3D reconstruction of the embryonic and fetal thigh muscles using multiple imaging modalities. The model created in this study is the first 4D atlas that follows thigh muscle development in human embryos and fetuses, and quantitative analysis of the model shows musculature typical of human bipedal walking. Further 4D studies of the MSS are required to elucidate the acquisition of locomotion in humans and to predict normal growth in order to detect congenital muscle disorders and anomalies. Applying our method to other parts of the body will be the focus of future studies to unravel the complicated process of morphological development in human embryos.

## DATA AVAILABILITY STATEMENT

The dataset generated during the current study is available from the corresponding author on reasonable request.

## ORCID

*Yutaka Yamaguchi* https://orcid.org/0000-0002-9171-8303
*Shigehito Yamada* https://orcid.org/0000-0002-8194-6927

## REFERENCES

Aronsson, D.D., Goldberg, M.J., Kling, T.F., Jr. & Roy, D.R. (1994) Developmental dysplasia of the hip. *Pediatrics*, 94(2 Pt 1), 201–208. https://doi.org/10.1542/peds.94.2.201

Bardeen, C.R. (1906) Development and variation of the nerves and the musculature of the inferior extremity and of the neighboring regions of the trunk in man. *American Journal of Anatomy*, 6(1), 259–390. https://doi.org/10.1002/aja.1000060108

Bardeen, C.R. & Lewis, W.H. (1901) Development of the limbs, body-wall and back in man. *American Journal of Anatomy*, 1(1), 1–35. https://doi.org/10.1002/aja.1000010102

Buckingham, M., Bajard, L., Chang, T., Daubas, P., Hadchouel, J., Meilhac, S. et al. (2003) The formation of skeletal muscle: from somite to limb. *Journal of Anatomy*, 202(1), 59–68. https://doi.org/10.1046/j.1469-7580.2003.00139.x

Castiello, U. & Parma, V. (2018) Fetal kinematics: basic outcomes and translational outlook. *ACS Chemical Neuroscience*, 9(2), 165–166. https://doi.org/10.1021/acschemneuro.8b00016

Charles, J.P., Suntaxi, F. & Anderst, W.J. (2019) In vivo human lower limb muscle architecture dataset obtained using diffusion tensor imaging. *PLoS One*, 14(10), e0223531. https://doi.org/10.1371/journal.pone.0223531

Christ, B. & Brand-Saberi, B. (2002) Limb muscle development. *The International Journal of Developmental Biology*, 46(7), 905–914.

de Vries, J.I. & Fong, B.F. (2006) Normal fetal motility: an overview. *Ultrasound in Obstetrics & Gynecology: The Official Journal of the International Society of Ultrasound in Obstetrics and Gynecology*, 27(6), 701–711. https://doi.org/10.1002/uog.2740

Delaurier, A., Burton, N., Bennett, M., Baldock, R., Davidson, D., Mohun, T.J. et al. (2008) The mouse limb anatomy atlas: an interactive 3D tool for studying embryonic limb patterning. *BMC Developmental Biology*, 8, 83. https://doi.org/10.1186/1471-213x-8-83

Diogo, R., Siomava, N. & Gitton, Y. (2019) Development of human limb muscles based on whole-mount immunostaining and the links between ontogeny and evolution. *Development*, 146(20), dev180349. https://doi.org/10.1242/dev.180349

Fedorov, A., Beichel, R., Kalpathy-Cramer, J., Finet, J., Fillion-Robin, J.C., Pujol, S. et al. (2012) 3D slicer as an image computing platform for the quantitative imaging network. *Magnetic Resonance Imaging*, 30(9), 1323–1341. https://doi.org/10.1016/j.mri.2012.05.001

Greiner, T.M. (2002) The morphology of the gluteus maximus during human evolution: prerequisite or consequence of the upright bipedal posture? *Human Evolution*, 17, 79–94. https://doi.org/10.1007/bf02436430

Hadlock, F.P., Harrist, R.B., Deter, R.L. & Park, S.K. (1982) Fetal femur length as a predictor of menstrual age: sonographically measured. *American Journal of Roentgenology*, 138(5), 875–878. https://doi.org/10.2214/ajr.138.5.875

Hadlock, F.P., Harrist, R.B., Carpenter, R.J., Deter, R.L. & Park, S.K. (1984) Sonographic estimation of fetal weight. The value of femur length in addition to head and abdomen measurements. *Radiology*, 150(2), 535–540. https://doi.org/10.1148/radiology.150.2.6691115

Hogervorst, T. & Vereecke, E.E. (2014) Evolution of the human hip. Part 2: muscling the double extension. *Journal of Hip Preservation Surgery*, 2(1), 3–14. https://doi.org/10.1093/jhps/hnu014

Huang, A.H. (2017) Coordinated development of the limb musculoskeletal system: tendon and muscle patterning and integration with the skeleton. *Developmental Biology*, 429(2), 420–428. https://doi.org/10.1016/j.ydbio.2017.03.028

Huang, A.H., Riordan, T.J., Pryce, B., Weibel, J.L., Watson, S.S., Long, F. et al. (2015) Musculoskeletal integration at the wrist underlies the modular development of limb tendons. *Development*, 142(14), 2431–2441. https://doi.org/10.1242/dev.122374

Ishida, H. (1972) On the muscular composition of lower extremities of apes based on the relative weight. *Journal of the Anthropological Society of Nippon*, 80(2), 125–145. https://doi.org/10.1537/ase1911.80.125

Ito, J. (1996) Morphological analysis of the human lower extremity based on the relative muscle weight. *Okajimas Folia Anatomica Japonica*, 73(5), 247–251. https://doi.org/10.2535/ofaj1936.73.5_247

Kanahashi, T., Yamada, S., Tanaka, M., Hirose, A., Uwabe, C., Kose, K. et al. (2016) A novel strategy to reveal the latent abnormalities in human embryonic stages from a large embryo collection. *Anatomical Record*, 299(1), 8–24. https://doi.org/10.1002/ar.23281

Kurjak, A., Vecek, N., Hafner, T., Bozek, T., Funduk-Kurjak, B. & Ujevic, B. (2002) Prenatal diagnosis: what does four-dimensional ultrasound add? *Journal of Perinatal Medicine*, 30(1), 57–62. https://doi.org/10.1515/JPM.2002.008

Lieberman, D.E., Raichlen, D.A., Pontzer, H., Bramble, D.M. & Cutright-Smith, E. (2006) The human gluteus maximus and its role in running. *Journal of Experimental Biology*, 209(11), 2143–2155. https://doi.org/10.1242/jeb.02255

Lu, Y., Yang, T., Luo, H., Deng, F., Cai, Q., Sun, W. et al. (2016) Visualization and quantitation of fetal movements by real-time three-dimensional ultrasound with live xPlane imaging in the first trimester of pregnancy. *Croatian Medical Journal*, 57(5), 474–481. https://doi.org/10.3325/cmj.2016.57.474

Lüchinger, A.B., Hadders-Algra, M., van Kan, C.M. & de Vries, J.I. (2008) Fetal onset of general movements. *Pediatric Research*, 63(2), 191–195. https://doi.org/10.1203/pdr.0b013e31815ed03e

Matsuda, Y., Ono, S., Otake, Y., Handa, S., Kose, K., Haishi, T. et al. (2007) Imaging of a large collection of human embryo using a super-parallel MR microscope. *Magnetic Resonance in Medical Sciences: MRMS: An Official Journal of JAPAN Society of Magnetic Resonance in Medicine*, 6(3), 139–146. https://doi.org/10.2463/mrms.6.139

Nishimura, H., Takano, K., Tanimura, T. & Yasuda, M. (1968) Normal and abnormal development of human embryos: first report of the analysis of 1,213 intact embryos. *Teratology*, 1(3), 281–290. https://doi.org/10.1002/tera.1420010306

Nowlan, N.C. (2015) Biomechanics of foetal movement. *European Cells & Materials*, 29, 1–21. https://doi.org/10.22203/eCM.v029a01

Okada, M., Morimoto, M. & Kimura, T. (1996) Mobility of hindlimb joints in Japanese macaques (Macaca fuscata) as influenced by biarticular musculature. *Folia Primatologica; International Journal of Primatology*, 66(1–4), 181–191. https://doi.org/10.1159/000157193

O'Rahilly, R. & Gardner, E. (1975) The timing and sequence of events in the development of the limbs in the human embryo. *Anatomy and Embryology*, 148(1), 1–23. https://doi.org/10.1007/bf00315559

Pooh, R.K., Shiota, K. & Kurjak, A. (2011) Imaging of the human embryo with magnetic resonance imaging microscopy and high-resolution transvaginal 3-dimensional sonography: human embryology in the 21st century. *American Journal of Obstetrics and Gynecology*, 204(1), 77.e1–77.e16. https://doi.org/10.1016/j.ajog.2010.07.028

Rodríguez, J.I., Garcia-Alix, A., Palacios, J. & Paniagua, R. (1988a) Changes in the long bones due to fetal immobility caused by neuromuscular disease. A radiographic and histological study. *The Journal of Bone and Joint Surgery*, 70(7), 1052–1060. https://doi.org/10.2106/00004623-198870070-00014

Rodríguez, J.I., Palacios, J., García-Alix, A., Pastor, I. & Paniagua, R. (1988b) Effects of immobilization on fetal bone development. A morphometric study in newborns with congenital neuromuscular diseases with intrauterine onset. *Calcified Tissue International*, 43(6), 335–339. https://doi.org/10.1007/bf02553275

Schneider, C.A., Rasband, W.S. & Eliceiri, K.W. (2012) NIH image to ImageJ: 25 years of image analysis. *Nature Methods*, 9(7), 671–675. https://doi.org/10.1038/nmeth.2089

Smith, B.R., Johnson, G.A., Groman, E.V. & Linney, E. (1994) Magnetic resonance microscopy of mouse embryos. *Proceedings of the National Academy of Sciences of the United States of America*, 91(9), 3530–3533. https://doi.org/10.1073/pnas.91.9.3530

Smith, B.R., Linney, E., Huff, D.S. & Johnson, G.A. (1996) Magnetic resonance microscopy of embryos. *Computerized Medical Imaging and Graphics*, 20(6), 483–490. https://doi.org/10.1016/s0895-6111(96)00046-8

Stalling, D., Westerhoff, M. & Hege, H.-C. (2005) Amira: a highly interactive system for visual data63 analysis. In: *The visualization handbook*. Amsterdam: Elsevier, pp. 749–767. https://doi.org/10.1016/b978-012387582-2/50040-x

Suzuki, Y., Matsubayashi, J., Ji, X., Yamada, S., Yoneyama, A., Imai, H. et al. (2019) Morphogenesis of the femur at different stages of normal human development. *PLoS One*, 14(8), e0221569. https://doi.org/10.1371/journal.pone.0221569

Tickle, C. (2015) How the embryo makes a limb: determination, polarity and identity. *Journal of Anatomy*, 227(4), 418–430. https://doi.org/10.1111/joa.12361

Verbruggen, S.W., Kainz, B., Shelmerdine, S.C., Hajnal, J.V., Rutherford, M.A., Arthurs, O.J. et al. (2018) Stresses and strains on the human fetal skeleton during development. *Journal of the Royal Society Interface*, 15(138), 20170593. https://doi.org/10.1098/rsif.2017.0593

Warmbrunn, M.V., de Bakker, B.S., Hagoort, J., Alefs-de Bakker, P.B. & Oostra, R.J. (2018) Hitherto unknown detailed muscle anatomy in an 8-week-old embryo. *Journal of Anatomy*, 233(2), 243–254. https://doi.org/10.1111/joa.12819

Wilde, S., Feneck, E.M., Mohun, T.J. & Logan, M. (2021) 4D formation of human embryonic forelimb musculature. *Development*, 148(4), dev194746. https://doi.org/10.1242/dev.194746

Yamaguchi, Y. & Yamada, S. (2018) The Kyoto collection of human embryos and fetuses: history and recent advancements in modern methods. *Cells, Tissues, Organs*, 205(5–6), 314–319. https://doi.org/10.1159/000490672

Yamaguchi, Y., Miyazaki, R., Kamatani, M., Uwabe, C., Makishima, H., Nagai, M. et al. (2018) Three-dimensional models of the segmented human fetal brain generated by magnetic resonance imaging. *Congenital Anomalies*, 58(2), 48–55. https://doi.org/10.1111/cga.12229

Yoneyama, A., Yamada, S. & Takeda, T. (2011) Fine biomedical imaging using X-ray phase-sensitive technique. In: Gargiulo, G. (Ed.) *Advanced biomedical engineering*. Rijeka: InTech, pp. 107–128. https://doi.org/10.5772/20456

Zihlman, A.L., McFarland, R.K. & Underwood, C.E. (2011) Functional anatomy and adaptation of male gorillas (Gorilla gorilla gorilla) with comparison to male orangutans (Pongo pygmaeus). *Anatomical Record*, 294(11), 1842–1855. https://doi.org/10.1002/ar.21449

Ziylan, T. & Murshid, K.A. (2003) An assessment of femur growth parameters in human fetuses and their relationship to gestational age. *Turkish Journal of Medical Sciences*, 33, 27–32.

## SUPPORTING INFORMATION

Additional supporting information can be found online in the Supporting Information section at the end of this article.